ANALYSIS OF THE NONLINEAR FORCING IN THE BI-GLOBAL RESOLVENT FORMULATION FOR A SELF-SIMILAR ADVERSE PRESSURE GRADIENT TURBULENT BOUNDARY LAYER AT THE VERGE OF SEPARATION

Bihai Sun, Kevin Liu, Antonio Matas, Callum Atkinson, Julio Soria
Laboratory for Turbulence Research in Aerospace & Combustion (LTRAC)
Department of Mechanical and Aerospace Engineering
Monash University
Clayton Victoria 3800, Australia
bihai.sun@monash.edu

ABSTRACT

This paper investigates the nonlinear forcing in the bi-global resolvent formulation for an self-similar adverse pressure gradient turbulent boundary layer (SS-APG-TBL) at the verge of separation. The analysis is based on time-resolved direct numerical simulation data, from which the forcing terms, defined as the mean-removed fluctuating Reynolds-stress gradients, are evaluated and Fourier transformed in both the spanwise direction and time. The forcing is examined through frequency–wavenumber spectra integrated over the wall-normal direction and through wall-normal–spanwise spectra evaluated over the peak forcing frequency range. The results show that the nine Reynolds-stress gradient terms have broadly comparable amplitudes, with terms sharing the same gradient direction exhibiting similar spectral organisation. The three total forcing components also display similar magnitudes and spectral shapes after self-similar scaling. All three attain their maxima at $\lambda_z/\delta_1 = 0.1$ and $\omega\delta_1/U_e = 35$. This peak differs markedly from both the maximum resolvent gain, which occurs at lower frequency and longer spanwise wavelength, and the Reynolds-stress spectra, which attain their maxima at larger spanwise wavelengths. The wall-normal analysis further shows that the forcing reaches its maximum near $y/\delta_1 = 1.2$, farther from the wall than the Reynolds-stress peak and coincident with the inflection point of the mean streamwise velocity profile. These findings show that the turbulent state in this flow is not governed by gain alone, and highlight the importance of the spectral and spatial organisation of the nonlinear forcing for reduced-order modelling and resolvent-informed flow control.

1 INTRODUCTION

Turbulent boundary layers subjected to adverse pressure gradient (APG) conditions are wall-bounded flows of fundamental theoretical interest and practical engineering relevance. Unlike zero pressure gradient (ZPG) boundary layers, APG flows depend strongly on upstream conditions, often referred to as history effects, which complicates systematic analysis. A notable exception is the SS-APG-TBL, in which the mean-velocity and Reynolds-stress profiles collapse when scaled with appropriate similarity variables, thereby eliminating history dependence. Following the work of Kitsios *et al.* (2017), complete self-similarity from the wall to the outer layer is achieved only at the verge of separation, where viscous effects become negligible. The SS-APG-TBL therefore provides an idealised yet physically realisable framework for investigating the mechanisms underlying adverse-pressure-gradient effects in wall-bounded turbulence.

Resolvent analysis has emerged as a powerful framework for identifying amplification mechanisms and coherent structures in turbulent shear flows by recasting the Navier–Stokes equations as a linear input–output system (McKeon & Sharma, 2010). In this formulation, the linearised operator about a given base flow is forced by nonlinear interactions, and the most amplified forcing and response modes are obtained through singular value decomposition (SVD) of the resolvent operator. While classical local resolvent analysis assumes spatial homogeneity and is therefore suited to parallel or weakly non-parallel flows, a bi-global formulation is required when streamwise and wall-normal inhomogeneities must be retained. This is particularly important for the SS-APG-TBL, where the boundary-layer thickness grows rapidly and parallel-flow approximation breaks down (Soria *et al.*, 2024). The bi-global approach retains both streamwise and wall-normal dependence while assuming homogeneity only in the spanwise direction, providing a more complete description of the linear amplification mechanisms in such flows.

Previous studies have predominantly focused on leading resolvent modes and their connection to observed flow structures, while comparatively less attention has been given to the statistical properties of the nonlinear forcing terms. Yet, characterising this forcing is crucial for connecting linear input–output analysis with the nonlinear dynamics that sustain turbulence.

The present study addresses this need by analysing the nonlinear forcing within a bi-global resolvent framework applied to an SS-APG-TBL at the verge of separation. High-resolution, time-resolved direct numerical simulation (DNS) data enable computation of the forcing terms from the fluctuating Reynolds-stress gradients with spatio-temporal detail not attainable using large-eddy simulation or experimental techniques. The forcing is examined from two complementary perspectives: frequency–wavenumber spectra integrated over the wall-normal direction, and wall-normal–spanwise spectra evaluated over the peak forcing frequency range. By analysing these spectra in light of the amplification characteristics of the resolvent operator and the Reynolds-stress response spectra, this study provides further physical insight into the dynamics of the SS-APG-TBL. The paper focuses on the spectral and spatial characteristics of the nonlinear forcing in the bi-global resolvent framework, while a more detailed presentation of the broader analysis is given by Sun *et al.* (2026).

2 BI-GLOBAL RESOLVENT ANALYSIS AND DIRECT NUMERICAL SIMULATION DATABASE

The analysis presented in this paper builds on the bi-global resolvent analysis framework developed for the SS-APG-TBL by Soria *et al.* (2024) and Gomez & McKeon (2025). The formulation is only summarised here for completeness. We adopt a three-dimensional Cartesian coordinate system in which $x_1 = x$ denotes the streamwise direction, $x_2 = y$ the wall-normal direction, and $x_3 = z$ the spanwise direction. The instantaneous velocity vector is $u = (u_1, u_2, u_3) = (u, v, w)$, and the pressure field is denoted by p. The spanwise wavenumber is $k_3 = k_z$, with associated wavelength $\lambda_z = \lambda_3 = 2\pi/k_3$.

In this framework, the fluctuating velocity and pressure fields are related to the nonlinear forcing through the resolvent operator, $\mathscr{H}_{k_3,\omega}$, as

$$\widehat{q}(x_1,x_2;k_3,\omega) = \begin{bmatrix} \widehat{u_1'}(x_1,x_2;k_3,\omega) \\ \widehat{u_2'}(x_1,x_2;k_3,\omega) \\ \widehat{u_3'}(x_1,x_2;k_3,\omega) \\ \widehat{p'}(x_1,x_2;k_3,\omega) \end{bmatrix} = \mathscr{H}_{k_3,\omega} \widehat{f}(x_1,x_2;k_3,\omega), \tag{1}$$

where $\widehat{(\cdot)}$ denotes the Fourier transform in both time and the spanwise direction, and

$$\widehat{q} = \left[\widehat{u_1'}, \widehat{u_2'}, \widehat{u_3'}, \widehat{p'}\right]^{\mathsf{T}} \tag{2}$$

is the response vector. The bi-global formulation retains both streamwise and wall-normal inhomogeneity while assuming homogeneity only in the spanwise direction. This is essential for the SS-APG-TBL, in which the boundary-layer thickness grows rapidly and parallel-flow approximations break down (Soria *et al.*, 2024; Gomez & McKeon, 2025).

The resolvent operator $\mathscr{H}_{k_3,\omega}$ is obtained by linearising the incompressible Navier–Stokes equations about the mean velocity field and inverting the resulting linear operator,

$$\mathscr{H}_{k_3,\omega} = \begin{bmatrix} \widehat{D}_{k_3,\omega} + \dfrac{\partial U_1}{\partial x_1} & \dfrac{\partial U_1}{\partial x_2} & 0 & \dfrac{\partial}{\partial x_1} \\ \dfrac{\partial U_2}{\partial x_1} & \widehat{D}_{k_3,\omega} + \dfrac{\partial U_2}{\partial x_2} & 0 & \dfrac{\partial}{\partial x_2} \\ 0 & 0 & \widehat{D}_{k_3,\omega} & ik_3 \\ \dfrac{\partial}{\partial x_1} & \dfrac{\partial}{\partial x_2} & ik_3 & 0 \end{bmatrix}^{-1}, \tag{3}$$

where

$$\widehat{D}_{k_3,\omega} \equiv -i\omega + U_1 \frac{\partial}{\partial x_1} + U_2 \frac{\partial}{\partial x_2} - \frac{1}{Re}\left(\frac{\partial^2}{\partial x_1^2} + \frac{\partial^2}{\partial x_2^2} - k_3^2\right), \tag{4}$$

with $U_1(x_1,x_2)$ and $U_2(x_1,x_2)$ denoting the mean streamwise and wall-normal velocity components, respectively.

For each wavenumber–frequency pair (k_3,ω), singular value decomposition of $\mathscr{H}_{k_3,\omega}$ yields forcing modes ϕ_i, response modes ψ_i, and gains σ_i,

$$\mathscr{H}_{k_3,\omega} = \sum_i \sigma_i \, \psi_i \, \phi_i^*. \tag{5}$$

Although the detailed modal structure is not the primary focus of the present paper, the gains and modes provide useful context for interpreting the nonlinear forcing spectra, which is presented and discussed by Soria *et al.* (2024).

The nonlinear forcing term in the bi-global resolvent formulation is defined as

$$\widehat{f}(x_1,x_2;k_3,\omega) = -\begin{bmatrix} \widehat{f_1} \\ \widehat{f_2} \\ \widehat{f_3} \\ 0 \end{bmatrix}. \tag{6}$$

The forcing components are defined as

$$\widehat{f_i} = \frac{\partial}{\partial x_j}\left(\widehat{u_i'u_j' - \overline{u_i'u_j'}}\right), \qquad i = 1,2,3. \tag{7}$$

Here, primes denote fluctuations about the mean, overbars denote temporal averaging, and repeated indices imply summation according to Einstein notation. The fourth component of $\widehat{f}$ is identically zero, corresponding to the pressure equation. To discuss the individual contributions to the forcing, we use the notation

$$\widehat{\phi_{\alpha\beta}} = \frac{\partial}{\partial x_\beta}\left(\widehat{u_\alpha' u_\beta' - \overline{u_\alpha' u_\beta'}}\right), \qquad \alpha,\beta = 1,2,3, \tag{8}$$

so that

$$\widehat{f_i} = \widehat{\phi_{i1}} + \widehat{\phi_{i2}} + \widehat{\phi_{i3}}. \tag{9}$$

These nine Reynolds-stress gradient terms represent the full tensor structure of the nonlinear forcing and form the focus of the present analysis.

The database employed in this study originates from a high-fidelity, time-resolved DNS of an SS-APG-TBL at the verge of separation. The simulation methodology and validation of self-similarity were reported by Kitsios *et al.* (2016), who showed that the flow is self-similar within a domain of interest (DOI) through streamwise constancy of the self-similar parameters and the collapse of first- and second-order statistical moments after normalisation with the self-similar scaling variables. The time-resolved dataset used here was generated using the same computational method and code described by Kitsios *et al.* (2017). The temporal sampling was refined relative to the earlier databases to enable temporal spectral analysis across the frequency range of interest. The key simulation parameters are summarised in Table 1.

In this study, the characteristic length and velocity scales are the displacement thickness and the external free-stream velocity, defined using the mean spanwise vorticity (Kitsios *et al.*, 2017). The displacement thickness is given by

$$\delta_1(x) = \frac{-1}{U_e}\int_0^{y_s} y\,\Omega_z(x,y)\,\mathrm{d}y, \tag{10}$$

and the external velocity is given by

$$U_e(x) = -\int_0^{y_s} \Omega_z(x,y)\,\mathrm{d}y, \tag{11}$$

where $\Omega_z(x,y)$ is the mean spanwise vorticity and y_s is the wall-normal position at which $\Omega_z(x,y)$ is 0.2% of the mean spanwise vorticity at the wall. Because the flow is self-similar within the DOI, the forcing spectra can be scaled using the local similarity variables and averaged in the streamwise direction.

Table 1: Summary of key DNS parameters in the DOI. N_x, N_y, and N_z denote the number of grid points in the streamwise, wall-normal, and spanwise directions. δ_1 and δ_2 are the displacement and momentum thicknesses. β is the Clauser pressure-gradient parameter. $\overline{u_\tau}$ is the mean friction velocity averaged over the domain of interest, $\overline{C_f}$ is the mean skin-friction coefficient averaged over the domain of interest, and δt is the temporal sampling interval normalised by U_e and δ_1. All ranges correspond to values within the DOI.

Parameter	Value
N_x	1,001
N_y	1,000
N_z	2,048
Re_{δ_1}	22,182–28,789
Re_{δ_2}	9,857–12,101
β	39
$\overline{u_\tau}$	0.007
$\overline{C_f}$	3.9×10^{-4}
$\delta t \times (U_e/\delta_1)$	0.0151

3 SPECTRAL AND SPATIAL CHARACTERISTICS OF THE NONLINEAR FORCING

The nonlinear forcing terms are computed from the DNS database according to Equations (6) and (8). The mean-removed Reynolds-stress tensor components are constructed from the instantaneous velocity fields, Fourier transformed in the spanwise direction and in time, and differentiated in space to obtain the forcing terms. Streamwise and wall-normal derivatives are evaluated using a sixth-order compact Padé differentiation scheme, while spanwise derivatives are computed spectrally via multiplication by ik_3. The resulting forcing fields depend on two physical coordinates (x_1,x_2) and two spectral coordinates (k_3,ω). In the following, these four-dimensional fields are examined from two complementary perspectives.

3.1 FREQUENCY–WAVENUMBER SPECTRA OF THE FORCING TERMS

Figure 1 presents the pre-multiplied spectra of the nine forcing-term components, integrated over the wall-normal coordinate, scaled by self-similar variables and averaged in the streamwise direction,

$$F^{y}_{\alpha\beta}(k_3,\omega) = \frac{1}{N_x}\sum_x \left(\frac{\delta_1}{U_e^2}\int_0^\infty \left\langle \widehat{\phi_{\alpha\beta}}\widehat{\phi_{\alpha\beta}}^* \right\rangle \left(x_1,\eta;k_3,\omega\right)\mathrm{d}\eta\right), \tag{12}$$

as well as the integrated spectra of the three forcing components,

$$F^{y}_{\alpha}(k_3,\omega) = \frac{1}{N_x}\sum_x \left(\frac{\delta_1}{U_e^2}\int_0^\infty \left\langle \widehat{f_\alpha}\widehat{f_\alpha}^* \right\rangle \left(x_1,\eta;k_3,\omega\right)\mathrm{d}\eta\right), \tag{13}$$

where $\eta = y/\delta_1(x)$ is the wall-normal coordinate in self-similar variables, and $\langle\cdot\rangle$ denotes ensemble averaging. The results are presented as functions of the spanwise wavelength λ_z for ease of interpretation.

Several features emerge from this analysis. First, the streamwise normal-stress gradient term F^y_{11} exhibits the largest amplitude among the nine components, but its peak is only approximately twice that of the weakest term, F^y_{22}. Second, terms sharing the same gradient direction, represented by the second index in $F^y_{\alpha\beta}$, exhibit similar spectral structure. Streamwise-gradient terms display the highest amplitudes and the broadest distributions in λ_z, spanwise-gradient terms are more narrowly concentrated around specific wavelengths, and wall-normal-gradient terms consistently exhibit the weakest amplitudes. Third, the three total forcing components F^y_1, F^y_2 and F^y_3, shown in the bottom row of Figure 1, display similar magnitudes and spectral shapes after self-similar scaling.

All three forcing components attain their maxima at $\lambda_z/\delta_1 = 0.1$ and $\omega\delta_1/U_e = 35$. This peak differs markedly from the resolvent gain maximum, which occurs at $\lambda_z/\delta_1 = 0.8$ and $\omega\delta_1/U_e < 0.2$, and from the Reynolds-stress spectra, which peak at $\lambda_z/\delta_1 = 1.0$–1.5. The spectral mismatch between forcing, gain and response indicates that the turbulence in this flow is not dominated by the highest-gain resolvent modes. Instead, modes with lower individual gains but stronger forcing appear to contribute more substantially to the observed turbulent state.

3.2 WALL-NORMAL–SPANWISE STRUCTURE AT THE PEAK FREQUENCY

To examine the spatial organisation of the nonlinear forcing, Figure 2 presents the wall-normal–spanwise distribution of the forcing terms at the peak frequency identified in Figure 1. Specifically, we plot

$$F^{\omega_\mathrm{p}}_{\alpha\beta}(k_3,y) = \frac{1}{N_x}\sum_x \left(\frac{\delta_1}{U_e^2}\int_{32U_e/\delta_1}^{37U_e/\delta_1} \left\langle \widehat{\phi_{\alpha\beta}}\widehat{\phi_{\alpha\beta}}^* \right\rangle \left(x_1,y;k_3,\omega\right)\mathrm{d}\omega\right), \tag{14}$$

and

$$F^{\omega_\mathrm{p}}_{\alpha}(k_3,y) = \frac{1}{N_x}\sum_x \left(\frac{\delta_1}{U_e^2}\int_{32U_e/\delta_1}^{37U_e/\delta_1} \left\langle \widehat{f_\alpha}\widehat{f_\alpha}^* \right\rangle \left(x_1,y;k_3,\omega\right)\mathrm{d}\omega\right), \tag{15}$$

where the frequency window $32 \le \omega\delta_1/U_e \le 37$ is centred on the forcing peak. The results are again presented as functions of the spanwise wavelength $\lambda_z = 2\pi/k_3$.

The wall-normal analysis confirms and extends the findings from the frequency–wavenumber spectra. The term $F^{\omega_\mathrm{p}}_{11}$ exhibits the largest amplitude, with a peak approximately 2.5 times that of the weakest term, $F^{\omega_\mathrm{p}}_{22}$. Terms sharing the same spatial-derivative direction display qualitatively similar organisation in the y–λ_z plane, irrespective of the Reynolds-stress component involved. The three total forcing components $F^{\omega_\mathrm{p}}_{1}$, $F^{\omega_\mathrm{p}}_{2}$ and $F^{\omega_\mathrm{p}}_{3}$ also exhibit comparable spatial distributions and similar peak amplitudes.

All forcing components attain maximum amplitude near $y/\delta_1 = 1.2$, which lies farther from the wall than the peaks in

Reynolds stresses at $y/\delta_1 \approx 1.0$. Notably, $y/\delta_1 = 1.2$ coincides with the inflection point of the mean streamwise velocity profile. This indicates that the strongest nonlinear forcing is organised around the inflectional region of the mean flow. The forcing is concentrated at $\lambda_z/\delta_1 = 0.1$, which is substantially smaller than the dominant scales observed in the velocity spectra and is consistent with the peak location identified in Figure 1.

3.3 RELATION BETWEEN FORCING, GAIN AND RESPONSE

The results above reveal a clear spectral separation between the nonlinear forcing, the resolvent gain, and the energetic turbulent response. The three forcing components attain their maxima at $\lambda_z/\delta_1 = 0.1$ and $\omega\delta_1/U_e = 35$, whereas the maximum resolvent gain occurs at $\lambda_z/\delta_1 = 0.8$ and $\omega\delta_1/U_e < 0.2$. These forcing scales also differ substantially from the dominant Reynolds-stress spectra, which peak at $\lambda_z/\delta_1 = 1.0$–1.5. The detailed gain distribution and representative mode shapes of the bi-global resolvent operator for this flow are presented by Soria *et al.* (2024). The observed turbulent state is therefore not determined by gain alone, because the strongest forcing and the strongest linear amplification occur in different regions of spectral space.

These observations also have implications for reduced-order modelling and, potentially, for flow control. If the dominant turbulent response were governed only by the highest-gain modes, control strategies based solely on gain optimisation might be expected to be most effective. The present results suggest that, for the SS-APG-TBL at the verge of separation, the forcing distribution must also be taken into account. In particular, the concentration of forcing at shorter spanwise wavelength, higher temporal frequency, and in the outer region near the mean-velocity inflection point points to a spectral and spatial region that may be especially relevant when formulating resolvent-informed modelling or control strategies.

4 CONCLUSIONS

This paper has examined the nonlinear forcing in the bi-global resolvent formulation for an SS-APG-TBL at the verge of separation using time-resolved DNS data. The forcing terms were evaluated from the mean-removed Reynolds-stress gradients and analysed from two complementary perspectives: frequency–wavenumber spectra integrated in the wall-normal direction, and wall-normal–spanwise spectra evaluated over the peak forcing frequency range.

The frequency–wavenumber analysis showed that the nine Reynolds-stress gradient terms have broadly comparable amplitudes, with the strongest term exceeding the weakest by only a moderate factor. Terms sharing the same gradient direction exhibit similar spectral organisation, while the three total forcing components display similar magnitudes and spectral shapes after self-similar scaling. All three forcing components attain their maxima at $\lambda_z/\delta_1 = 0.1$ and $\omega\delta_1/U_e = 35$.

Comparison with the resolvent gain and the Reynolds-stress spectra reveals a clear spectral mismatch between forcing, gain and response. The forcing peak occurs at substantially shorter spanwise wavelength and higher temporal frequency than the gain maximum, while also differing from the dominant Reynolds-stress scales. This indicates that the turbulent state in the present flow is not governed by gain alone, and that the spectral organisation of the nonlinear forcing plays a central role in determining which resolvent mechanisms are most active in practice.

The wall-normal–spanwise analysis further showed that all forcing components attain their maximum amplitude near $y/\delta_1 = 1.2$, farther from the wall than the Reynolds-stress peak and coincident with the inflection point of the mean streamwise velocity profile. The strongest forcing is therefore concentrated in the outer region of the flow and organised around the inflectional region of the mean profile.

Overall, these results provide new physical insight into the spectral and spatial organisation of the nonlinear forcing in the SS-APG-TBL at the verge of separation. They also suggest that both the amplification characteristics of the resolvent operator and the distribution of the nonlinear forcing should be considered in future reduced-order modelling and resolvent-informed flow-control strategies.

Acknowledgments

This work was supported by an Australian Research Council Discovery Project grant. The authors acknowledge computational resources provided by the Pawsey Supercomputing Centre (supported by the Australian and Western Australian Governments) and the National Computational Infrastructure (NCI, supported by the Australian Government), allocated through the National Computational Merit Allocation Scheme (NCMAS) and the Monash University–NCI partnership scheme.

REFERENCES

Gomez, Salvador R. & McKeon, Beverley J. 2025 Linear analysis characterizes pressure gradient history effects in turbulent boundary layers. *Journal of Fluid Mechanics* **1002**, A20.

Kitsios, V., Atkinson, C., Sillero, J. A., Borrell, G., Gungor, A. G., Jiménez, J. & Soria, J. 2016 Direct numerical simulation of a self-similar adverse pressure gradient turbulent boundary layer. *International Journal of Heat and Fluid Flow* **61**, 129–136.

Kitsios, V., Sekimoto, A., Atkinson, C., Sillero, J. A., Borrell, G., Gungor, A. G., Jiménez, J. & Soria, J. 2017 Direct numerical simulation of a self-similar adverse pressure gradient turbulent boundary layer at the verge of separation. *Journal of Fluid Mechanics* **829**, 392–419.

McKeon, B. J. & Sharma, A. S. 2010 A critical-layer framework for turbulent pipe flow. *Journal of Fluid Mechanics* **658**, 336–382.

Soria, J., Matas, A., Liu, K., Gomez, S. R., Jaroslawski, T. & McKeon, B. J. 2024 Biglobal resolvent analysis of a self-similar adverse pressure gradient turbulent boundary layer at the verge of separation. In *Center for Turbulence Research Proceedings of the Summer Program 2024*.

Sun, B., Liu, K., Matas, A., Atkinson, C. & Soria, J. 2026 Characterization of the fluctuating Reynolds-stress gradients and their implications for bi-global resolvent analysis in an adverse-pressure-gradient turbulent boundary layer. *Journal of Physics: Conference Series* (in press).

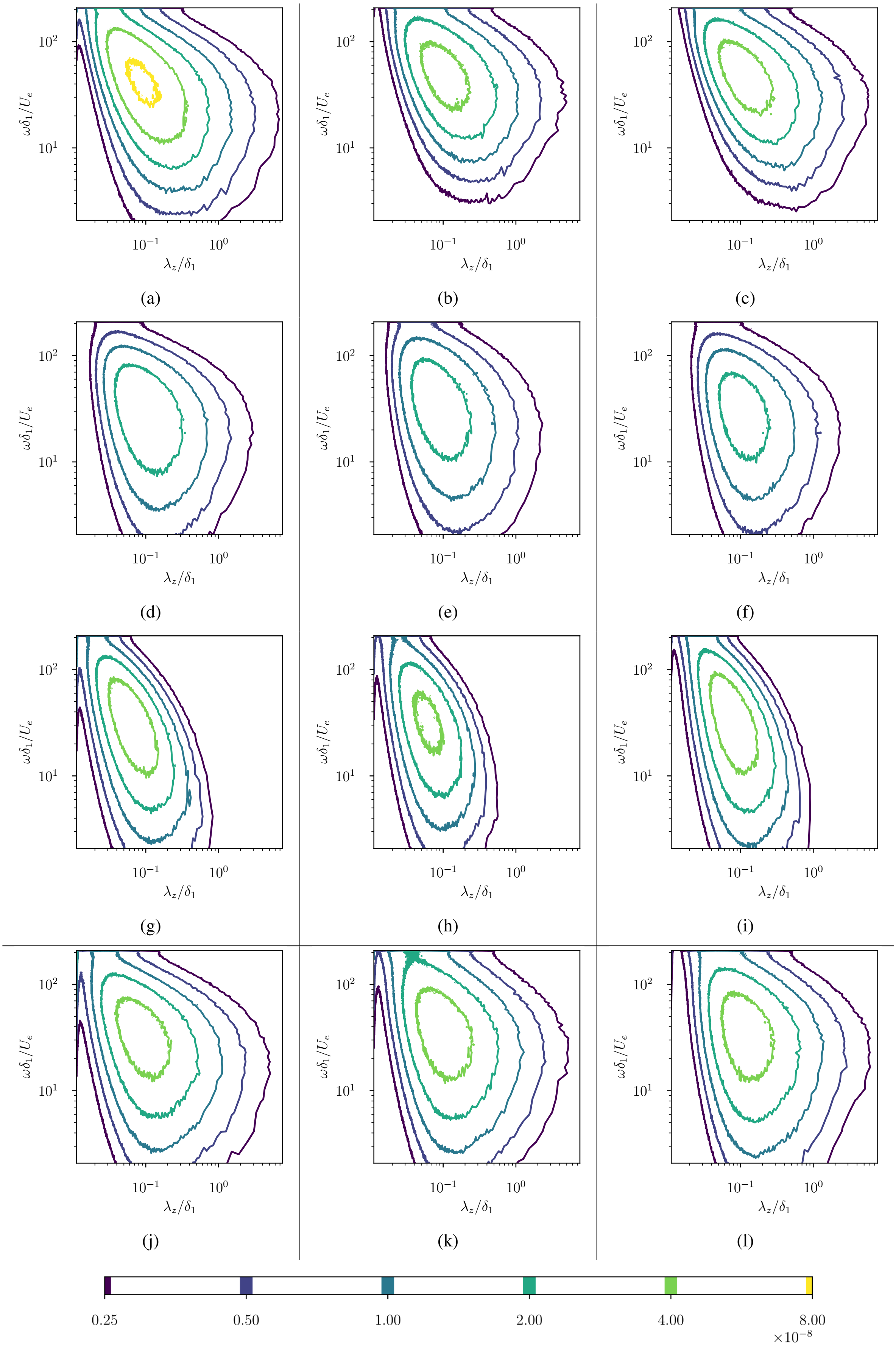

Figure 1: Pre-multiplied frequency–wavelength spectra of the forcing terms, integrated in the wall-normal direction and averaged in the streamwise direction: (a)–(c) F^y_{11}, F^y_{21}, F^y_{31}; (d)–(f) F^y_{12}, F^y_{22}, F^y_{32}; (g)–(i) F^y_{13}, F^y_{23}, F^y_{33}; (j)–(l) F^y_1, F^y_2, F^y_3. Each forcing component in panels (j)–(l) is composed of the three terms above it in the same column. Contour levels are on a logarithmic scale with ratio 0.5.

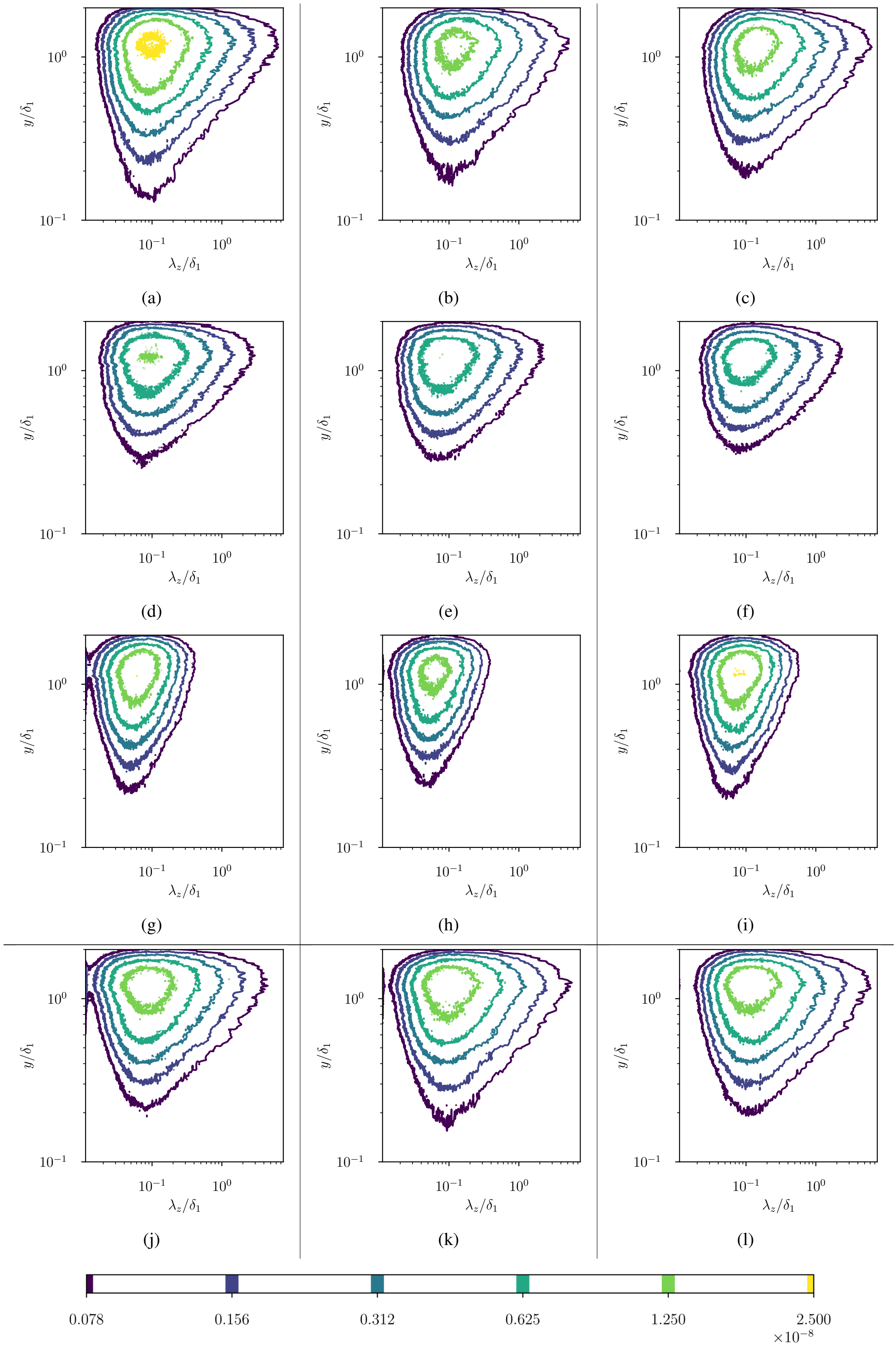

Figure 2: Pre-multiplied spectra in the wall-normal–spanwise plane at the peak temporal frequency range, $32 \leq \omega\delta_1/U_e \leq 37$, averaged in the streamwise direction: (a)–(c) $F_{11}^{\omega_p}$, $F_{21}^{\omega_p}$, $F_{31}^{\omega_p}$; (d)–(f) $F_{12}^{\omega_p}$, $F_{22}^{\omega_p}$, $F_{32}^{\omega_p}$; (g)–(i) $F_{13}^{\omega_p}$, $F_{23}^{\omega_p}$, $F_{33}^{\omega_p}$; (j)–(l) $F_1^{\omega_p}$, $F_2^{\omega_p}$, $F_3^{\omega_p}$. Each forcing component in panels (j)–(l) is composed of the three terms above it in the same column. Contour levels are on a logarithmic scale with ratio 0.5.